

## Analysis of Vernier Scans during RHIC Run-13

A. Drees

October 2013

Collider Accelerator Department  
**Brookhaven National Laboratory**

**U.S. Department of Energy**

USDOE Office of Science (SC)

Notice: This technical note has been authored by employees of Brookhaven Science Associates, LLC under Contract No. DE-AC02-98CH10886 with the U.S. Department of Energy. The publisher by accepting the technical note for publication acknowledges that the United States Government retains a non-exclusive, paid-up, irrevocable, world-wide license to publish or reproduce the published form of this technical note, or allow others to do so, for United States Government purposes.

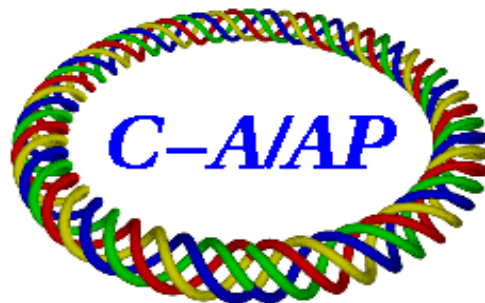
## **DISCLAIMER**

This report was prepared as an account of work sponsored by an agency of the United States Government. Neither the United States Government nor any agency thereof, nor any of their employees, nor any of their contractors, subcontractors, or their employees, makes any warranty, express or implied, or assumes any legal liability or responsibility for the accuracy, completeness, or any third party's use or the results of such use of any information, apparatus, product, or process disclosed, or represents that its use would not infringe privately owned rights. Reference herein to any specific commercial product, process, or service by trade name, trademark, manufacturer, or otherwise, does not necessarily constitute or imply its endorsement, recommendation, or favoring by the United States Government or any agency thereof or its contractors or subcontractors. The views and opinions of authors expressed herein do not necessarily state or reflect those of the United States Government or any agency thereof.

C-A/AP/488  
October 2013

# **Analysis of Vernier Scans during RHIC Run-13 (pp at 255 GeV/beam)**

**A. Drees**



**Collider-Accelerator Department  
Brookhaven National Laboratory  
Upton, NY 11973**

Notice: This document has been authorized by employees of Brookhaven Science Associates, LLC under Contract No. DE-AC02-98CH10886 with the U.S. Department of Energy. The United States Government retains a non-exclusive, paid-up, irrevocable, world-wide license to publish or reproduce the published form of this document, or allow others to do so, for United States Government purposes.

# Analysis of Vernier Scans during RHIC Run-13 (pp at 255 GeV/beam)

A. Drees

October 16, 2013

## 1 Introduction

At RHIC the collision rate per IP is measured by the Zero Degree Calorimeters (ZDC) [1]. Both, STAR and PHENIX, contain those detectors that are of identical design but are equipped with different Photo Multiplier Tubes (PMT) and operated with individually different HV setups and also slightly different read-out electronics. The collision rate, as measured by the ZDC, corresponds to the rate of mutual forward neutral particles above a variable threshold and within a certain coincidence window. Due to the differences in the detector electronics the two devices are calibrated individually every year by the use of vernier scans [2].

During the RHIC polarized proton Run in 2013 a total of 6 vernier scans per experiment were performed. This note presents the data and summarizes the results, i.e. effective ZDC cross section and emittance measurements, from those scans.

## 2 Vernier Scan Technique

fill	beam moved in (IP6/IP8)	date	fill pattern	# coll. pairs (IP6/IP8)	lattice
17198	(B/B)	03-09-13	28x28	(26/28)	pp13e-s4
17263	(Y/Y)	03-23-13	109x109	(100/107)	pp13e-s4
17341	(B/B)	04-08-13	109x109	(100/107)	pp13b-s1
17416	(B/Y)	04-23-13	111x110	(101/110)	pp13b-s1
17479	(Y/Y)	05-09-13	111x111	(102/111)	pp13b-s1
17600	(Y/Y)	06-07-13	111x111	(102/111)	pp13b-s1

Table 1: List of fills with vernier scans during the 2013 run.

The transverse size and shape of the beam overlap region is measured by recording the interaction rate as a function of the transverse beam separation. A fit of the measured interaction rate as a function of the separation allows to determine the effective beam size, and thus the emittance, as well as the maximum achievable collision rate and the effective cross section of the detector in use. Typically additional effects such as a possible crossing

angle or the hourglass effect require correction factors to be applied. Two different lattices, listed in Table 1 and both with an approximate value of  $\beta^* = 0.65$  m (from model), were used during the run. However, actual  $\beta^*$  values used later in this note are measured [3] ones and not taken from the model. The beam energy of 255 GeV corresponds to  $\gamma = 271.6$ . Table 1 lists the fills with vernier scans, the date and some basic parameters.

## 2.1 The Fit Function

The shape of the overlap region, i.e. the collision rate  $R_{coll}(x)$  as a function of distance between the two beams,  $x$ , is mapped by the vernier scan and can usually best be described by a single Gauss-function:

$$R_{coll}(x) = R_{Bkgd} + R_{max} \times \exp\left(\frac{-(x - x_0)^2}{2 \sigma_x^2}\right) \quad (1)$$

with the 4 free parameters:

$R_{Bkgd}$ : non-collision related background signal in the collision rate

$R_{max}$ : maximum collision rate seen by the ZDC detector (corrected for background)

$x_0$ : location of the maximum

$\sigma_x$ : width of the overlap region

The application and DAQ software that supports fully automated vernier scans at STAR and PHENIX employs single-Gauss fits for its online analysis [4].

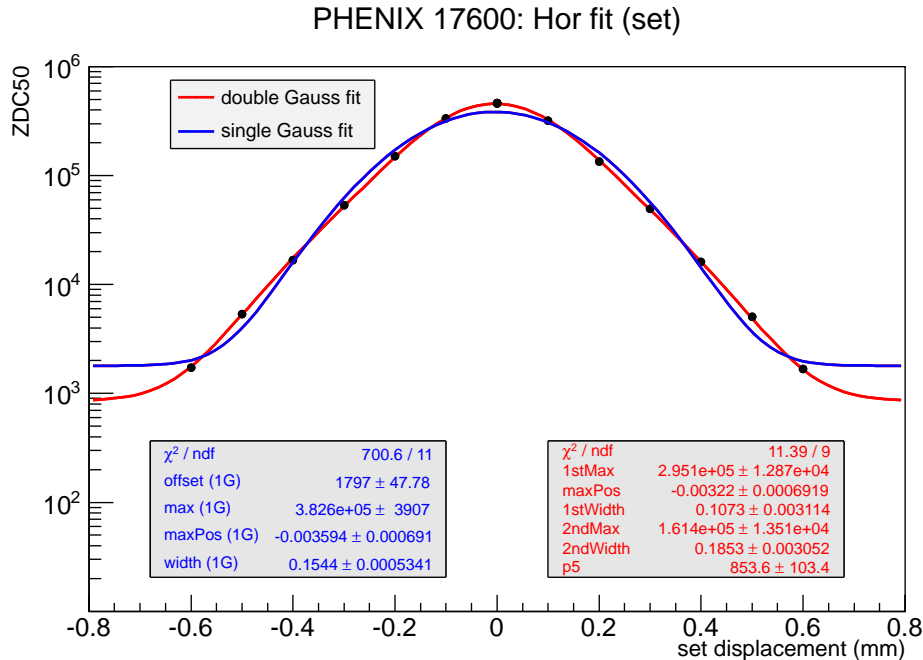


Figure 1: Horizontal data from a vernier scan in fill 17600 at the PHENIX experiment fitted with a 1-Gauss and a 2-Gauss fit function. The 2-Gauss fit function is clearly favored by about a factor 50 in  $\chi^2/\text{ndf}$

However, in the case of proton beams at 255 GeV, the single Gauss approach does no

longer fit the data (as shown in Figure 1) and a double Gauss-function is chosen:

$$R_{\text{coll}}(x) = R_{\text{max},1} \times \exp\left(\frac{-(x-x_0)^2}{2\sigma_{x,1}^{\text{VS}}}\right) + R_{\text{max},2} \times \exp\left(\frac{-(x-x_0)^2}{2\sigma_{x,2}^{\text{VS}}}\right) \quad (2)$$

The double Gauss function has 5 free parameters:

$R_{\text{max},1}$ : maximum collision rate of the core region

$x_0$ : location of both the maxima

$\sigma_{x,1}$ : width of the core overlap region

$R_{\text{max},2}$ : maximum of the tail distribution

$\sigma_{x,2}$ : width of the tail region

The double Gauss approach is not needed to describe the data for protons at 100 GeV nor for Heavy Ions and its necessity was first observed during Run-9 [5]. I assume that both Gauss distributions, core and tail, are centered around the same location  $x_0$ . All data from Run-13 was fitted with the double Gauss even in cases when the  $\chi^2/\text{ndf}$  for the single Gauss fit was not quite as large as in Figure 1 and in the single digit range.

### 3 The Effective Cross Section

The effective detector cross section  $\sigma_{\text{ZDC}}^{\text{eff}}$  of a detector, in this case the ZDCs, can be determined by the beam current, the collision rate and the overlap region  $\sigma_{x,y}^{\text{VS}}$  of the two beams. The maximum collision rate and the width of the overlap region are derived from the fits to the vernier scan data.

$$\sigma_{\text{ZDC}}^{\text{eff}} = \frac{R_{\text{max}} 2\pi n_B n_Y \sigma_x^{\text{VS}} \sigma_y^{\text{VS}}}{n_{\text{coll}} f_{\text{rev}} N_B N_Y} \quad (3)$$

where:

$R_{\text{max}}$  = maximum collision rate seen by the ZDC detector (corrected for background)

$n_B, n_Y$  = number of blue and yellow bunches respectively

$\sigma_{x,y}^{\text{VS}}$  = RMS beam-overlap size, derived from the fit to the vernier scan data

$n_{\text{coll}}$  = number of colliding bunch pairs in the IP where the ZDC detector is located

$f_{\text{rev}}$  = revolution frequency, approx. 78.4 kHz

$N_{B,Y}$  = total number of blue and yellow protons, from DCCT

Figure 2 shows one example of a vernier scan, here in the vertical plane in IP6, moving the yellow beam. The top graph depicts the ZDC coincidence rate as a function of the set value, the bottom depicts the ZDC coincidence rate as a function of the measured distance of the two beams. Both are fitted with a double Gauss-function according to Equation 2. The  $\chi^2/\text{ndf}$  in the top graph (using set values from the model) reaches 2 and is thus slightly larger than in the bottom graph (using measured distances), demonstrating that using the measured displacements (i.e. data from the DX BPMs) yields better fit results. This is the case for most scans in Run-13. The beam overlap size  $\sigma^{\text{VS}}$  in Equation 3 is given by the combination of the two widths from the double Gauss fit. The combined width adds the two individual widths according to their amplitudes:

$$\sigma_{x,y}^{\text{comb}} = \sigma_1^{x,y} \frac{R_{\text{max},1}}{R_{\text{max},1} + R_{\text{max},2}} + \sigma_2^{x,y} \frac{R_{\text{max},2}}{R_{\text{max},1} + R_{\text{max},2}} \quad (4)$$

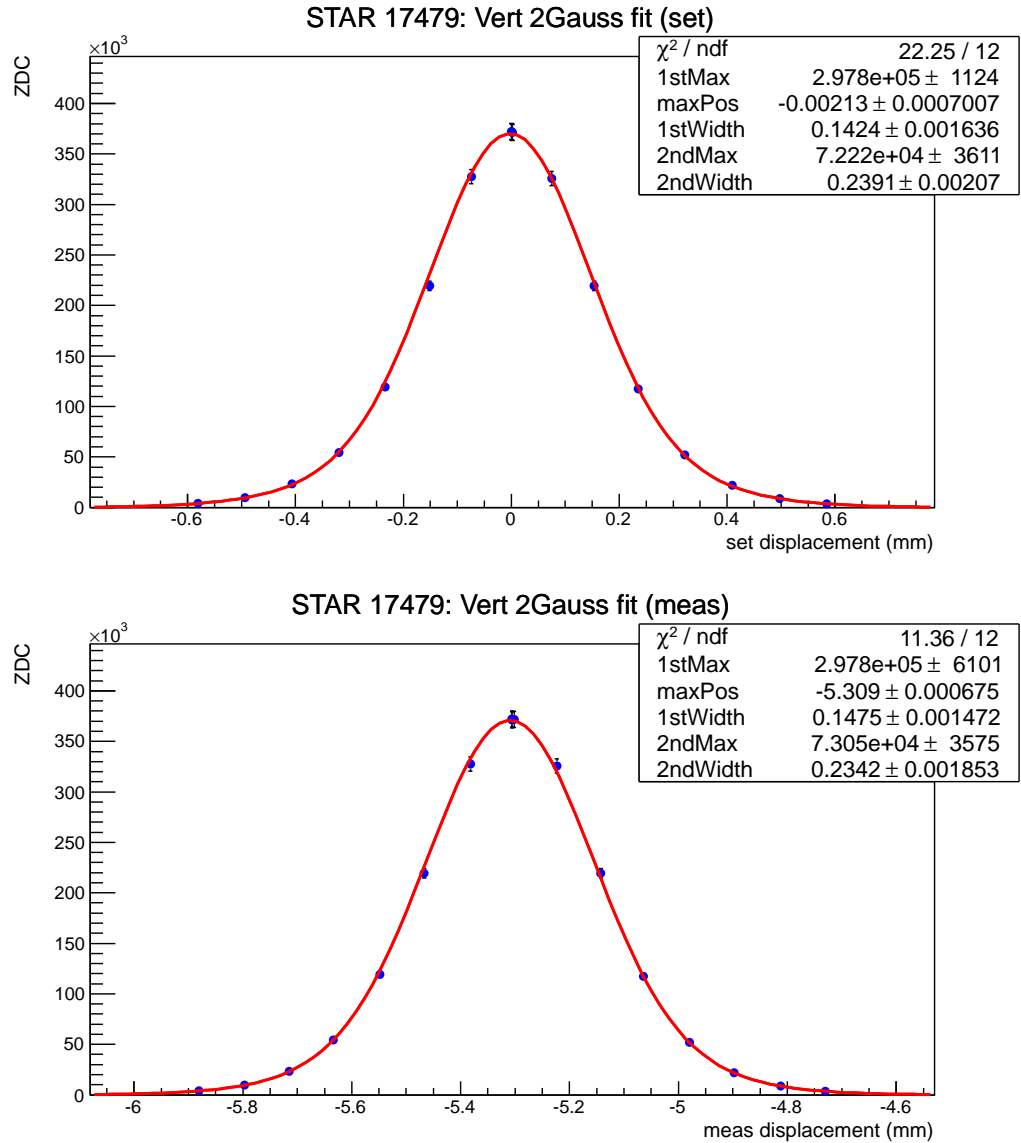


Figure 2: Data from a vertical vernier scan at IP6 in store 17479 (lattice pp13b-s1). Each data point corresponds to a measurement interval of 30 sec.

“x” and “y” refer to the two planes, while “1” and “2” refer to the core (1) and tail (2) part of the distribution respectively. Once the measured widths from the two approaches, using set or measured distances, are combined they agree to better than  $5 \mu\text{m}$ .

Several corrections apply to the cross section and/or emittance measurement using the vernier scan method. They affect the collision rate (accidental coincidences), the beam current measurement (fill pattern and debunched beam) and the measurement of the width (hour-glass, crossing angle, beam-beam, model inaccuracy). The various effects are outlined below.

## 4 Corrections

### 4.1 Beam Current and Fill Pattern

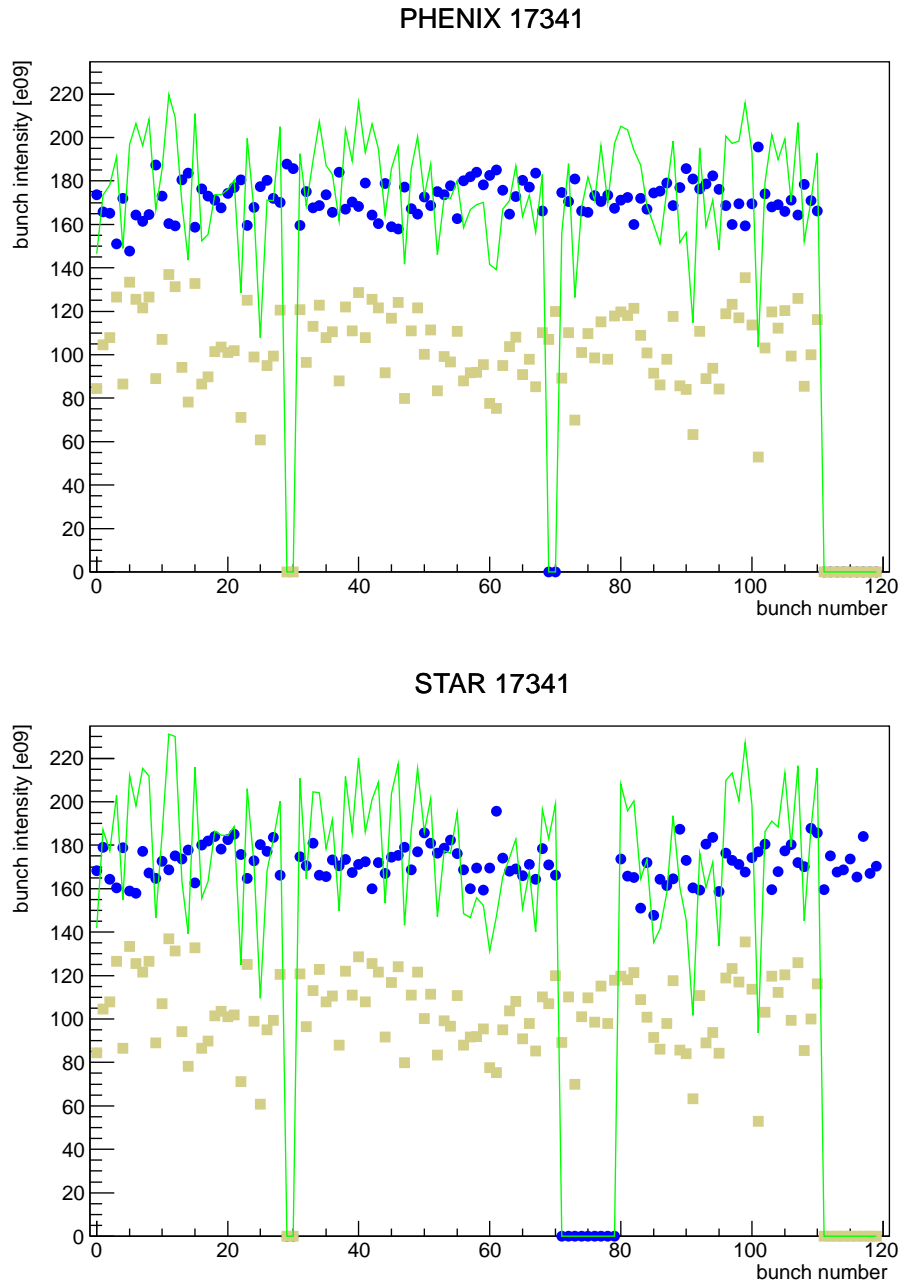


Figure 3: Fill pattern in fill 17341 at the time of the vernier scans. 17341 was filled with a 109x109 pattern. The blue and yellow symbols represent individual blue and yellow bunches, the green line corresponds to a scaled product of individual bunches.

The collision rate, i.e. the ZDC coincidence rate, is corrected for a change of the evolution of the beam current point-by-point. For this correction the total circulating

beam is used as measured by the DCCTs [6] while the measurements from the WCM [6] (total bunched beam) are ignored. This assumes that, with protons, all beam is bunched. While there is no ongoing debunching of proton beams during the store, beam could systematically debunch at the time of rebucketing (or caused by RF failures). Systematic and small bunched beam loss is difficult to measure since there is a habitual discrepancy between the WCM and the DCCT that changes when the WCM changes its gain setting (about 10 times per store) and the WCM measurement will change accordingly by up to 2% at times. Such automatic gain adjustments will also happen at the time of rebucketing. One cannot distinguish between a loss of bunched beam and the appearance of a change in beam current due to gain changes. Therefore the typical size of the change right after rebucketing is treated as a systematic error. For the stores with the vernier scans this virtual loss of bunched beam is between 0.5% and 1.5%. The systematic error assigned to this effect is 2 times 1% (for blue and yellow).

In Equation 3 the beam current in each bunch is given as the total number of protons per ring divided by the number of bunches in blue and yellow respectively:  $N_{\text{total}}/n_{B,Y}$ , thus using an average bunch intensity. This approach relies on a uniform distribution of the total beam over the bunches in the rings. Large bunch intensity fluctuations could potentially change the actual product depending on the colliding pairs of bunches and their individual intensities. The actual colliding pairs are different at the two IPs. Figure 3 shows the store with the largest fluctuations in the fill pattern.

The top graph shows the blue and yellow patterns respectively (blue and dark yellow symbols) as they are combined in IP8. The green line is the product of the individual pairs divided by 100 so it could be shown on the same scale. The bottom graph shows the equivalent data combining the bunches as they are paired in IP6 (blue is shifted by a third of the ring). In this worst case of the 6 fills with vernier scans, the actual product of the blue and yellow bunches would change by 1% in PHENIX if paired correctly, which is a negligible amount. Nevertheless a systematic error of 1% is assigned to the uncertainty caused by store to store variations of the fill pattern.

## 4.2 Accidental Coincidences

The collision rate, defined by the ZDC coincidences, is contaminated by false, or accidental, coincidence signals caused by high singles rates. Singles rates, i.e. the signal from just one side of the ZDC detector, contain a large amount from the coincidence signal and an even larger portion of unrelated signals that are typically from collisions but not from mutually forward neutral particles. The signal from the blue-incoming side is referred to as  $ZDC_B$ , and from the yellow-incoming side as  $ZDC_Y$ . A purely statistical approach to correct for accidental coincidences yields:

$$ZDC_{BY} = \frac{ZDC_B ZDC_Y n_{\text{coll}}}{n_B n_Y f_{\text{rev}}} \quad (5)$$

$$ZDC_{\text{corr}} = ZDC_{\text{raw}} - ZDC_{BY} \quad (6)$$

with the parameters equivalent to Equation 3 and  $ZDC_{\text{raw}}$  corresponding to the uncorrected collision rate. This approach overestimates the number of accidental coincidences by hits in the two sides of the ZDC detector that lead to coincidence hits but are not true beam crossing events. The following Equation corrects for multiple hits that are counted as a single hit and contains the correction for accidental hits from above [7]:

$$ZDC_{\text{log.corr}} = n_{\text{coll}} f_{\text{rev}} \left( -\ln \left( 1 - \frac{ZDC_{\text{raw}} - ZDC_{BY}}{n_{\text{coll}} f_{\text{ref}} + ZDC_{\text{raw}} - ZDC_B - ZDC_Y} \right) \right) \quad (7)$$

Figure 4 demonstrates the effect and amount of the two different corrections. The bottom

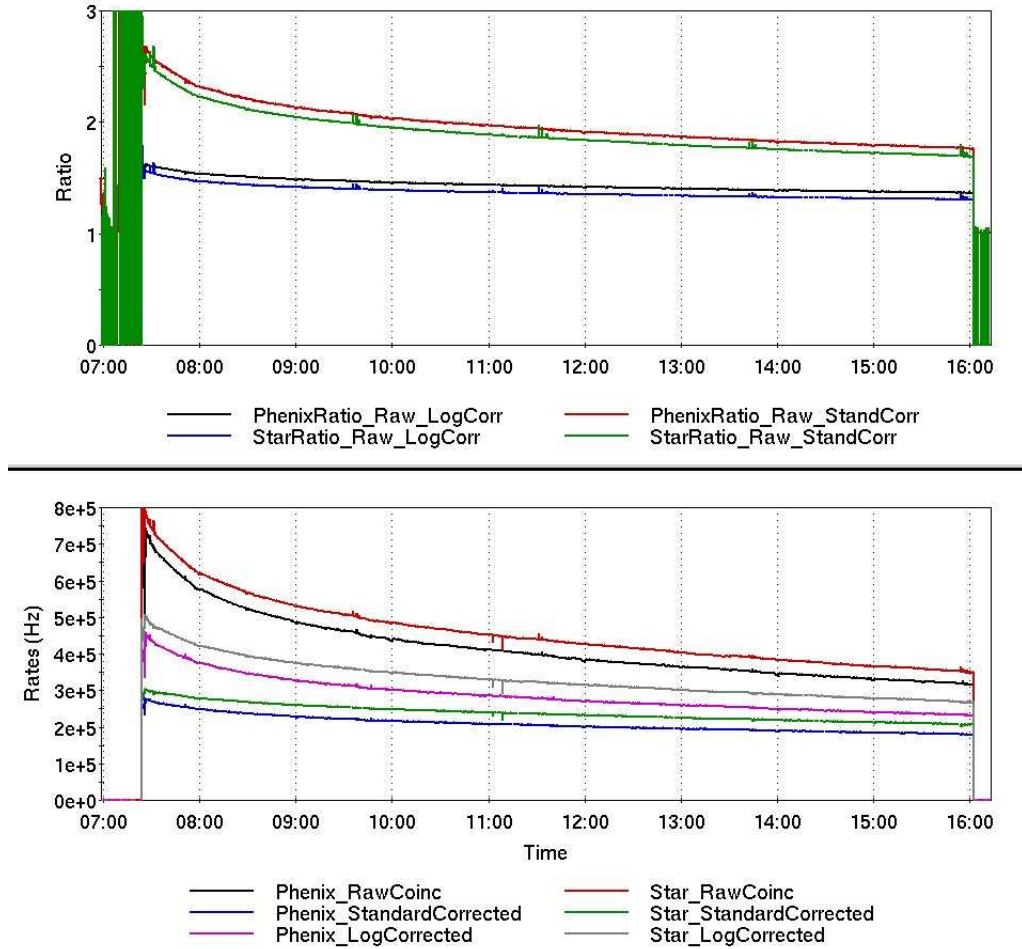


Figure 4: Bottom: Rates (“\_RawCoinc”) and corrected rates according to Eq. 6 (“\_StandardCorrected”) and Eq. 7 (“\_LogCorrected”) for both experiments in fill 17414, Apr 22 2013. Top: Ratios of the raw coincidence rates and the various corrected rates.

graph shows the uncorrected ZDC coincidence rates for the two experiments (“\_RawCoinc”), the coincidence rates corrected according to Eq. 6 (“\_StandardCorrected”) and the coincidence rates corrected using Eq. 7 (“\_LogCorrected”). The top graph presents the calculated ratios of the uncorrected coincidence rates and the LogCorrected rates (“Ratio\_Raw\_LogCorr”) as well as the ratio of uncorrected to StandardCorrected rates (“Ratio\_Raw\_StandCorr”). While the Ratio\_Raw\_LogCorr is almost constant around a factor 1.5, the standard correction scheme yields a factor of 2.5 at the start of a store and drops down to about a factor 2 at the end. This demonstrates the significant over-correction when using a purely statistical approach according to Eq. 6. Once the corrections are applied to both experimental coincidence signals, the ratio between the two experiments should be constant. However, the data comprises a remaining store to store variation in the order of 4%. Hence a 4% systematic error is assigned to the accidental correction.

### 4.3 BPMs

Beam position measurements rely on the BPMs [8], here in particular the DX BPMs which are attached to the DX magnets, approximately 8 m from the the Interaction Point (IP). DX BPMs are in a common beam pipe and subject to both beams. Q1 BPMs are dual plane BPMs just like the DX BPMs but in separate beam pipes and attached to the triplet quadrupoles Q1. They are about 25 m away from the IP.

#### 4.3.1 Beam Position at the IP

Issues of the beam position measurement systematically affect the measurement of the beam width. There are two components: relative and absolute measurements. BPMs appear reliable and accurate when used for relative measurements (i.e. step size in a vernier scan, see 4.3.2).

Unfortunately, in absolute terms the beam position measurement is difficult if not impossible to establish. The position of the two beams at the IP, provided they are in optimized head-on collisions, should give the same value regardless of which beam is measured. In principle, there are two devices available to extrapolate to the IP, the DX BPMs and the Q1 BPMs. The distance between the Q1 BPMs is 50.05 m in both IPs, and the distance between the DX BPMs is 16.32 m (IP6) and 16.65 m (IP8). There is only a drift between the DX BPMs but two horizontal dipoles (D0 and DX) between the two Q1 BPMs. DX BPMs have the extra difficulty - or advantage - that they are subject to both beams, hence any possible physical offset would apply to both beams and thus cancel out when the difference between the two beams is calculated. The position of the beam at the IP for one beam (blue or yellow) is given by

$$\text{Pos}_{\text{IP}} = \frac{1}{2} (\text{BPM}_{\text{in}} + \text{BPM}_{\text{out}}), \quad (8)$$

with “in” and “out” referring to the two sides of the IP (in-coming and out-going). The difference  $\Delta$  between the two beams according to the two devices (“DX” or “Q1”) then follows:

$$\Delta_{\text{device}} = \text{Pos}_{\text{IP}}^{\text{blue}} - \text{Pos}_{\text{IP}}^{\text{yellow}}, \quad (9)$$

where  $\text{Pos}_{\text{IP}}$  is calculated according to Equation 8 above and “device” refers to either DX BPM or Q1 BPM. This is done for the two planes and the two IPs separately. The results are summarized in Table 2 below.

The problem with these numbers is apparent. Taking the DX BPM measurements alone, the blue and yellow beams are separated by up to 150  $\mu\text{m}$  - while colliding head-on! Head-on collisions are guaranteed by the vernier scans and all data in Table 2 is taken right after a successful scan. In addition, the “fake” separation is not constant but varies from store to store, and also by up to 150  $\mu\text{m}$  (IP6, vertical plane). Therefore the uncertainty in the determination of the absolute beam position at the IP when using the DX BPM is at least as large as the largest measured “fake” separation, i.e. 150  $\mu\text{m}$ . Using a larger sample of fills rather than the 6 fills with vernier scans, might reveal even larger pseudo separations.

Due to the size of the position discrepancy between the two beams, the Q1 BPMs were also consulted in hopes of reducing the uncertainty. The results are also listed in Table 2. The first observation is that the alleged difference between the two beams as measured by the Q1 BPMs appears to be even larger, more than 1 mm, and that in the vertical plane, the plane without further optical elements between the two devices! Additionally, there

device	17198	17263	17341	17416	17479	17600
$\Delta_{DX}^H$ IP6	80	20	5	20	90	110
$\Delta_{Q1}^H$ IP6	-450	-450	-470	-490	-460	-430
$\Delta_{DX}^H$ IP8	75	55	50	60	80	75
$\Delta_{Q1}^H$ IP8	-120	-160	-130	-160	-80	-90
$\Delta_{DX}^V$ IP6	-55	10	-145	-25	-35	-70
$\Delta_{Q1}^V$ IP6	1360	1450	1400	1410	1410	1410
$\Delta_{DX}^V$ IP8	35	25	40	-25	-20	-20
$\Delta_{Q1}^V$ IP8	-1290	-1390	-1050	-1490	-1250	-1180

Table 2: Measurements of the difference of the blue and yellow beam position at the two IPs using DX and Q1 BPMs. Units are  $\mu\text{m}$ .

appears to be no correlation between the values from the Q1 BPMs and the DX BPMs. The Q1 BPMs are of no help in reducing the absolute uncertainty. The store to store variation alone is surprisingly large (up to  $230 \mu\text{m}$  in the vertical plane in IP8) indicating even more substantial problems with the data from the Q1 BPMs.

#### 4.3.2 Step size

For Run-13 the beam position “x” in both, Equations 1 and 2, is taken from the measured value (i.e. from the DX BPMs) when a vernier scan is performed. In order to study the reliability of the distance measurement, DX BPM data is compared to the set value from the model for each plane and ring for every individual vernier scan. Figure 5 shows one example. The data shown is taken during the vertical vernier scan 17479 in STAR. The top left and right graphs show the variations of the blue beam as seen by the DXB5V (left) and DXB6V (right) devices while the yellow beam is moved across the blue. Since the yellow beam was moved, the visible motion of the blue beam is caused by the beam-beam effect [5]. However small, the distance between the two beams in the IP is corrected for this additional motion point by point. The bottom left and right graphs show the movement of the yellow beam during the scan as seen by the sector 5 DX BPM (DxY5V) and the sector 6 DX BPM (DxY6V). In this particular case, DXY5V registers 10% more motion than asked for (i.e. an “over-shoot” of 110 measured microns for every 100 set microns) while DxY6V registers 1% less.

Using Equation 8 to extrapolate to the IP, in all vernier scans a consistent and reproducible few percent motion more than were asked for were measured. Consistency and reproducible in sign and amount indicate a systematic and non-statistical shift (“over-shoot”) in the distance measurements when comparing the model with the DX BPM data and thus confirm the reliability of the DX BPMs when used for relative measurements. The over-shoot applies to both planes, both IPs, both rings and lattices in slightly varying amounts:

**IP8** between 2.5% and 5% over-shoot, i.e. a requested value of 1 mm results in a measured value of 1.03 mm (on average). While the range is large, there is no consistent change with the switch from one lattice to the other nor between the planes.

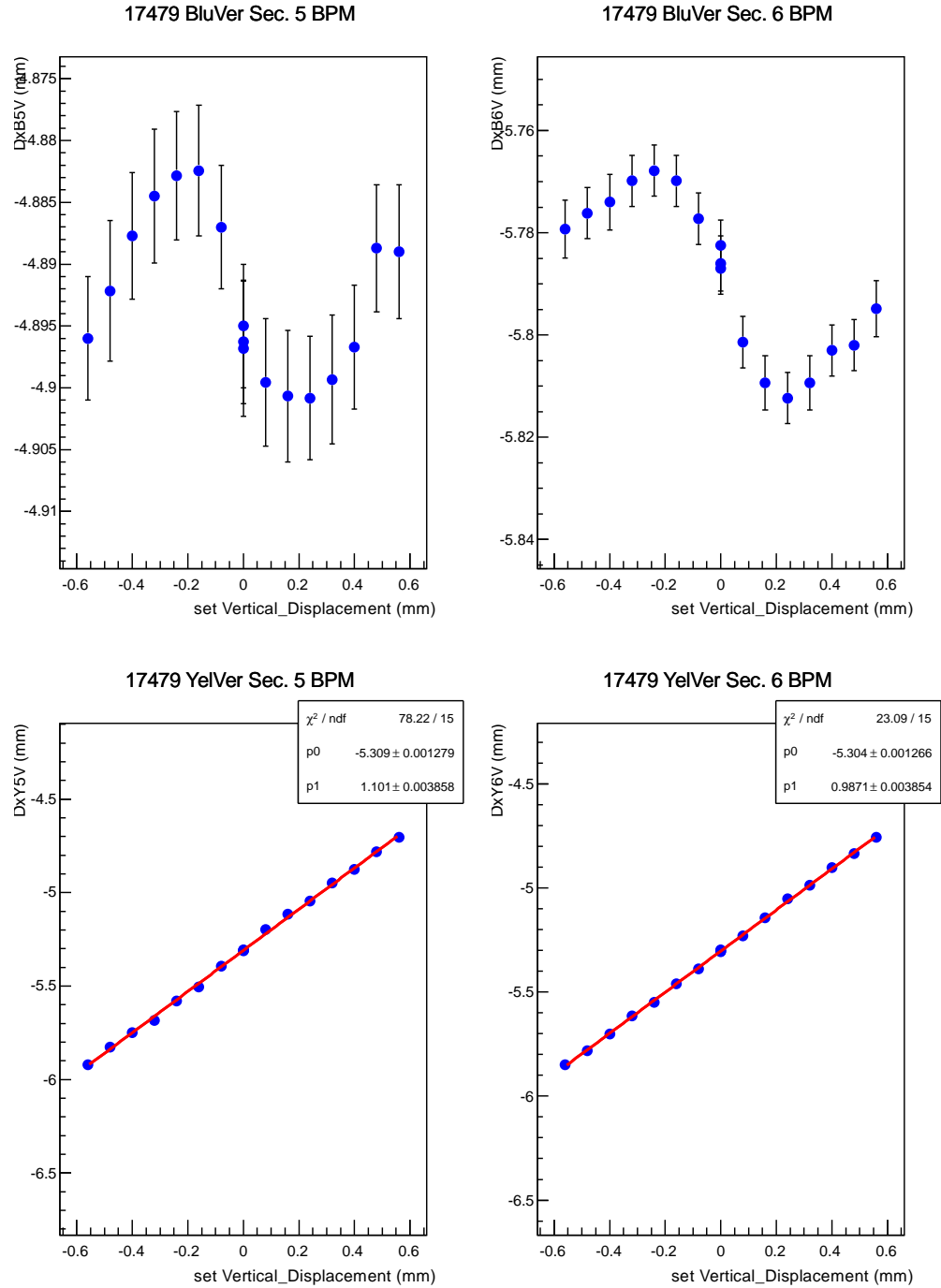


Figure 5: Measured beam positions as a function of set position (from model) during the vertical half of the vernier scan in IP6 during fill 17479. The yellow beam was moved.

**IP6** between 1.8% and 4.5 % over-shoot, smaller in the horizontal plane and the first lattice.

The store to store variation in the over-shoot within the same plane, ring and lattice is a

measure for the accuracy and reproducibility of the DX BPMs. Thus a systematic error of 2% is added to account for the uncertainty when using the BPMs to measure the distance between the two beams in a vernier scan.

### 4.3.3 Crossing Angles

Crossing angles can reduce the maximum collision rate to varying degrees depending on the bunch length. In order to determine this angle, all four DX BPMs in each plane on either side of the IP have to provide reliable and accurate absolute beam position measurements. Unfortunately very few data to prove the dependence of the collision rate on the crossing

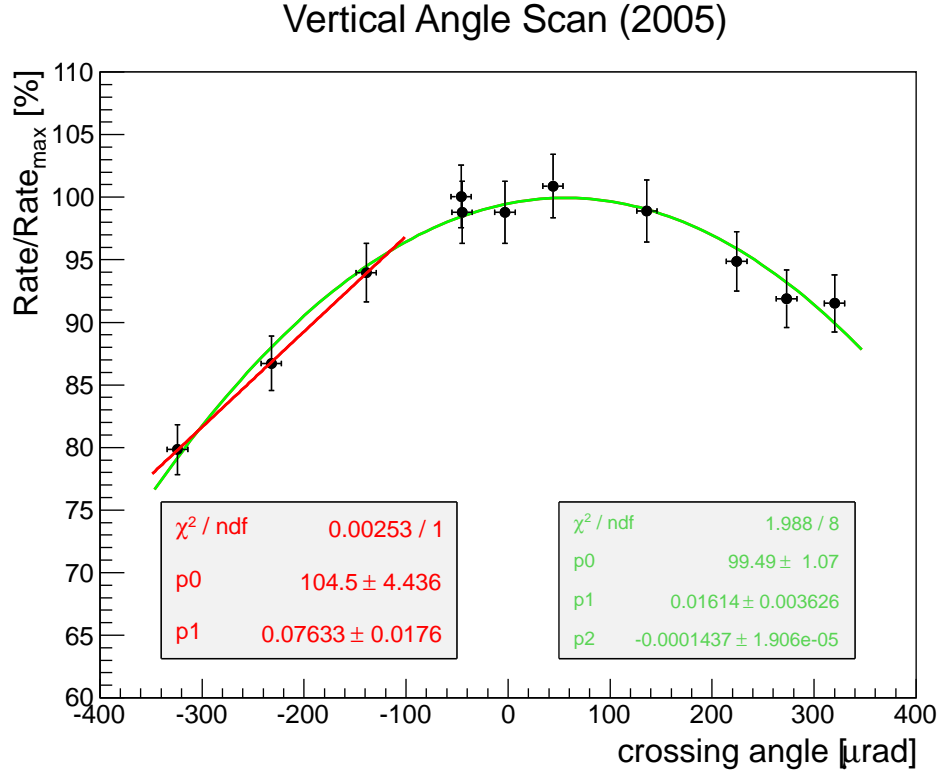


Figure 6: Relative change of collision rate in % as a function of the vertical crossing angle in IP8 in fill 7112 from Run-05.

angle is available and there is no complete scan from Run-13. One angle scan per run (energy and species) is recommendable. However, the measurement procedure is delicate and the risk of creating large backgrounds or of losing the beam in the process is relatively large. One example covering a significant range of angles is shown in Figure 6. The scan is from Run-5 and done with the yellow beam of polarized protons at 100 GeV. The angle is measured using the yellow DX BPMs in the PHENIX IP. It turns out that in this particular case the measured “0” is off by only 60  $\mu\text{rads}$ .

The scan covers a range of 0.7 dram and is fitted with a parabola (green line and fit parameters). For comparison, an area at the ‘shoulder’ of the distribution is fitted with a straight line (red line and fit parameters). In this area, a few hundred  $\mu\text{rad}$  away from perfectly aligned beams, the drop in the collision rate corresponds to approximately 0.76 % per 10  $\mu\text{rad}$  step. There is a similar range of data available from Run-13, shown in

Figure 7. No complete scan is available and the shown measurements were taken on one 'shoulder' of the distribution only, thus only a straight line fit could be applied (red line). Here, the drop in reference to the extrapolated maximum rate is linear and yields about

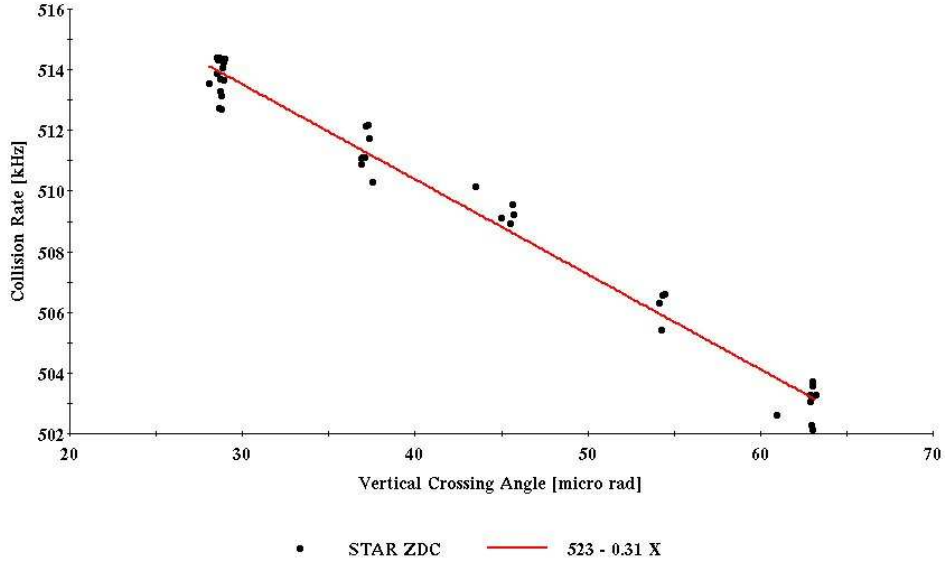


Figure 7: Collision rate at STAR as a function of the vertical crossing angle between the two beams in IP6 in fill 17479.

0.6 % per 10  $\mu\text{rad}$  step which is within less than 25% of the measurement from 2005, hence the conclusion that the data in Figure 7 is taken on the shoulder. The differences in the slopes are likely due to different bunch lengths at the time.

As outlined in section 4.3.1 the Q1 BPMs are of no help in determining the crossing angle and the DX BPMs disagree by at least 150  $\mu\text{m}$  at times corresponding to an uncertainty of about a 20  $\mu\text{rad}$  collision angle. Using this value as guidance and assuming a linear correlation (i.e. being in the 'shoulder' area), I assign an uncertainty of 1% that is associated with the lack of knowledge of the true crossing angles of the blue and yellow beams. Calculating the crossing angles from the DX and Q1 BPMs and taking their measurements at face value proved meaningless. However, the measured angles are listed in Table 3. Appearances here are the same as before (compare with Table 2). There is no correlation between the Q1 and DX BPM angle measurements, which is not surprising given that there was no correlation already for the position measurements. While the true collision angles cannot be measured, their presence at times is obvious (for example in Figure 7). However, the data does indicate that the typically present angles are likely smaller than a few hundred  $\mu\text{rad}$  and it supports an estimate of an additional systematic error of 1% resulting in a total of 2% due to crossing angles.

#### 4.4 Hourglass Reduction

The hourglass reduction factor  $R_{\text{hg}}$  [9] represents a loss in luminosity due to geometrical effects for Gaussian beams. The geometrical effect is caused by the parabolic shape of the beta-function along  $z$  in the IP between the triplet quadrupoles. For this note,  $R_{\text{hg}}$  was calculated using the "StoreAnalysis" application [10]. Typically this factor ranges from

device	17198	17263	17341	17416	17479	17600
Hor DX BPM IP6	-50	-30	-50	-10	20	-30
Hor Q1 BPM IP6	-50	-60	-90	-80	-80	-80
Hor DX BPM IP8	-60	-50	-10	0	-20	-30
Hor Q1 BPM IP8	-20	-30	-90	-50	-40	-50
Ver DX BPM IP6	-40	10	-70	0	-90	-120
Ver Q1 BPM IP6	-40	-70	-70	-30	-70	-80
Ver DX BPM IP8	-40	-10	30	0	30	40
Ver Q1 BPM IP8	-40	-70	30	0	40	-20

Table 3: Collision angles as measured by the DX and the Q1 BPMs (rounded to the nearest 10). Units are in  $\mu\text{rad}$ .

about 0.6 to 0.75 for protons at 255 GeV in RHIC for the two lattices that were used in 2013, depending on the bunch length (the longer the bunches the smaller the reduction factor). However, due to the distance of the ZDCs from the IP ( 20 m), this geometrical effect has no implication on the effective cross section for this particular detector. At this distance the beam size simply appears enlarged by the hourglass effect leading to a collision rate that is reduced but the true rate none-the-less. The measured effective cross section (see Eq. 3) is independent of the beta-function at the IP. The hourglass correction needs to be applied for emittance measurements though. The hourglass enlarged beam width, as seen by the ZDC detectors, has to be projected to the 'true' width at the IP with a known value of  $\beta^*$  to calculate the emittance.

## 5 Emittance Measurement

Given the RMS beam size one can calculate the normalized beam emittance  $\epsilon_{x,y}^{\text{RMS}}$  from vernier scans assuming that the beam sizes are the same in the two rings, and provided the beta functions at the IPs,  $\beta^*$ , in all 4 planes are known. The true beta-function in a given lattice can deviate significantly from the model. In 2013 the largest deviation at the IPs was measured to be 30% in the yellow horizontal plane at IP6 for the e-lens lattice pp13e-s4. Therefore, for this note, measured beta functions [3] were used to calculate the emittance from the measured beam sizes. The measured beam sizes and their model counterparts are listed in Table 4. Beam sizes measured by the vernier scan technique cannot distinguish between the two rings since they invariably measure the size of the overlap region only. Thus the  $\beta_{\text{blue}}^*$  and  $\beta_{\text{yellow}}^*$  values were combined into one effective  $\beta^*$  value per plane:

$$\beta_{\text{eff}}^* = \frac{1}{\sqrt{2}} \sqrt{(\beta_{\text{blue}}^*)^2 + (\beta_{\text{yellow}}^*)^2} \quad (10)$$

Using measured effective beta functions (according to Equation 10 and based on the measurements listed in Table 4) , the RMS normalized emittances can be derived from the vernier scans:

$$\epsilon_{x,y}^{\text{RMS}} = \left( \frac{\sigma_{x,y}^{\text{VS}}}{\sqrt{2}} \right)^2 \frac{1}{\beta_{\text{eff},x,y}^*} \gamma \quad (11)$$

lattice	STAR				PHENIX			
	BH	BV	YH	YV	BH	BV	YH	YV
pp13e-s4								
measured	0.69	0.67	0.81	0.61	0.66	0.65	0.68	0.62
model	0.68	0.62	0.62	0.62	0.65	0.74	0.67	0.74
pp13b-s1								
measured	0.74	0.82	0.60	0.62	0.63	0.77	0.79	0.75
model	0.64	0.63	0.66	0.67	0.61	0.64	0.60	0.68

Table 4: Model and measured beta-functions (taken from [3]) at IP6 and IP8 in units of [m].

with  $\gamma = 271.635$  for 255 GeV protons. Table 5 and Figure 8 summarize the various emittance measurements.

device	17198	17263	17341	17416	17479	17600
Hor VS IP6	2.6	3.2	5.4	4.0	3.3	3.0
Hor VS IP8	2.9	3.2	4.9	3.7	3.4	2.9
Hor IPM	2.5	3.4	4.5	3.4	2.9	3.0
Ver VS IP6	3.0	3.8	5.5	3.9	3.5	3.2
Ver VS IP8	3.2	3.7	5.0	3.7	3.3	3.0
Ver IPM	2.4	3.2	4.5	3.5	3.4	3.3
Hor VS IP6	101	113	135	123	109	100
Hor VS IP8	103	110	130	123	113	101
Ver VS IP6	102	113	144	123	117	108
Ver VS IP8	106	113	135	125	114	106

Table 5: Top: Measured RMS normalized emittance in units of mm dram. IPM emittance for the two rings were combined into one value equivalent to equation 10. Bottom: Measured RMS single beam sizes in the two IPs in units of  $\mu\text{m}$  and a statistical error of  $\pm 3 \mu\text{m}$ .

The IPM measurements [11] were supplied with a 10% error, the emittance measurements from the vernier scans with a 5% error. However, the errors of the IPM measurements are estimated at this point. The agreement in the horizontal plane is quite good with the exception of the third scan (fill 17341). This scan happened to be done with significantly larger transverse emittance than the other five. Here the IPM and the vernier scan disagree by about 20%. In the vertical plane, a similar size discrepancy appears not only for fill 17341 but also for the first two. Both were done with the first lattice, pp13b-s4. For this lattice, however, the measurement of the beta-function at the IPs and

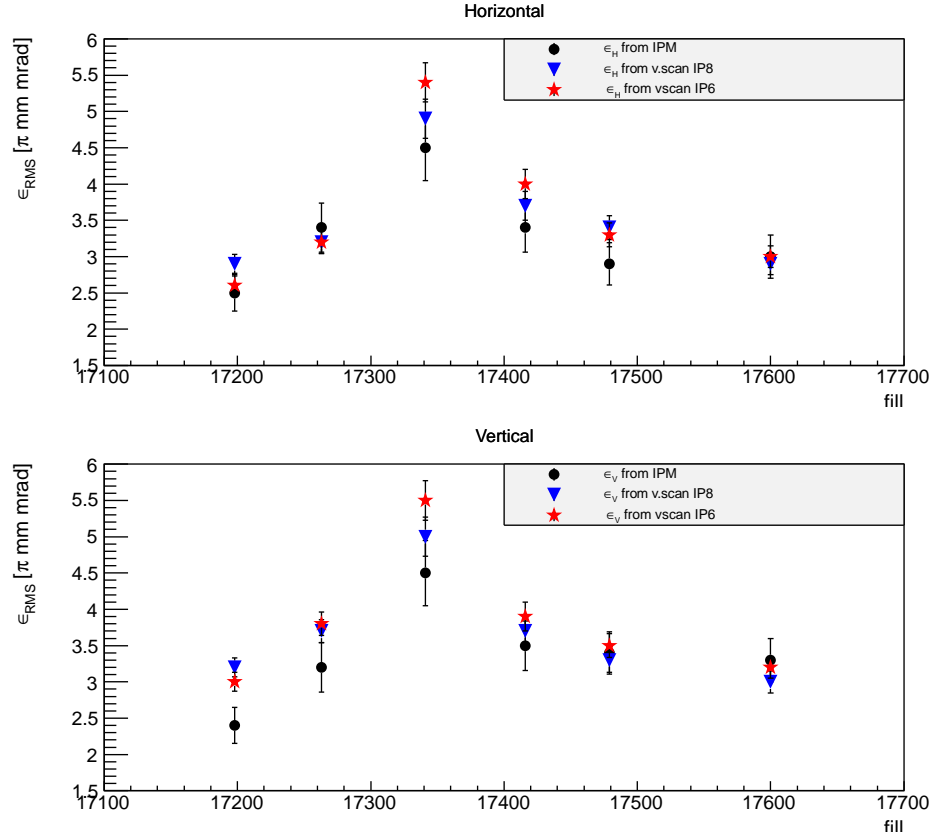


Figure 8: RMS emittance from IPM (blue and yellow combined) and from the vernier scans in IP8 and IP6.

the IPMs is less reliable since fewer data was available for analysis ([3]). To summarize, the measurements at the two IPs agree within 10% while the vernier scans and the IPMs differ by up to 20%. In most cases the IPM measured emittances are smaller than the ones resulting from a vernier scan.

## 6 Cross Section Results

The measured effective ZDC cross sections are summarized in Table 6 and shown in Figure 9. The corrections that were discussed above were applied in the table as well as in the plots. PHENIX signals were altered on Apr 3, 2013 and the results were combined for the two periods individually, before that date and after. The fit in Figure 9 (bottom) reflects this change in the experimental signals.

Both sets of cross section results, for IP6 and IP8, are consistent with statistical scatter. As a consistency check, the ratio of the luminosities in STAR and PHENIX is shown in Figure 10. Note that vernier scans are not done at the same time but one after the other, with a typical time delay of about 30 minutes between the two. The instantaneous luminosity of one or the other experiment needs to be scaled accordingly when ratios are computed. The ratio between the two experiments not only reflects the different numbers of colliding bunch pairs in the two experiments but also the different values of  $\beta^*$  in the

fill	STAR		PHENIX	
	$\sigma_{\text{eff}}^{\text{ZDC}} [\text{mbarn}]$	$\mathcal{L} [10^{32} \text{cm}^{-2} \text{s}^{-1}]$	$\sigma_{\text{eff}}^{\text{ZDC}} [\text{mbarn}]$	$\mathcal{L} [10^{32} \text{cm}^{-2} \text{s}^{-1}]$
17198	$2.73 \pm 0.14$	$0.17 \pm 0.01$	$2.59 \pm 0.13$	$0.18 \pm 0.01$
17263	$2.85 \pm 0.14$	$0.73 \pm 0.04$	$2.51 \pm 0.12$	$0.78 \pm 0.04$
17341	$2.93 \pm 0.20$	$0.60 \pm 0.03$	$2.18 \pm 0.11$	$0.68 \pm 0.03$
17416	$2.81 \pm 0.14$	$1.02 \pm 0.05$	$2.03 \pm 0.10$	$1.13 \pm 0.05$
17479	$2.71 \pm 0.13$	$1.37 \pm 0.07$	$2.07 \pm 0.10$	$1.46 \pm 0.07$
17600	$2.51 \pm 0.12$	$1.84 \pm 0.08$	$1.95 \pm 0.10$	$1.98 \pm 0.08$

Table 6: Effective cross sections and instantaneous luminosities at the two IPs.

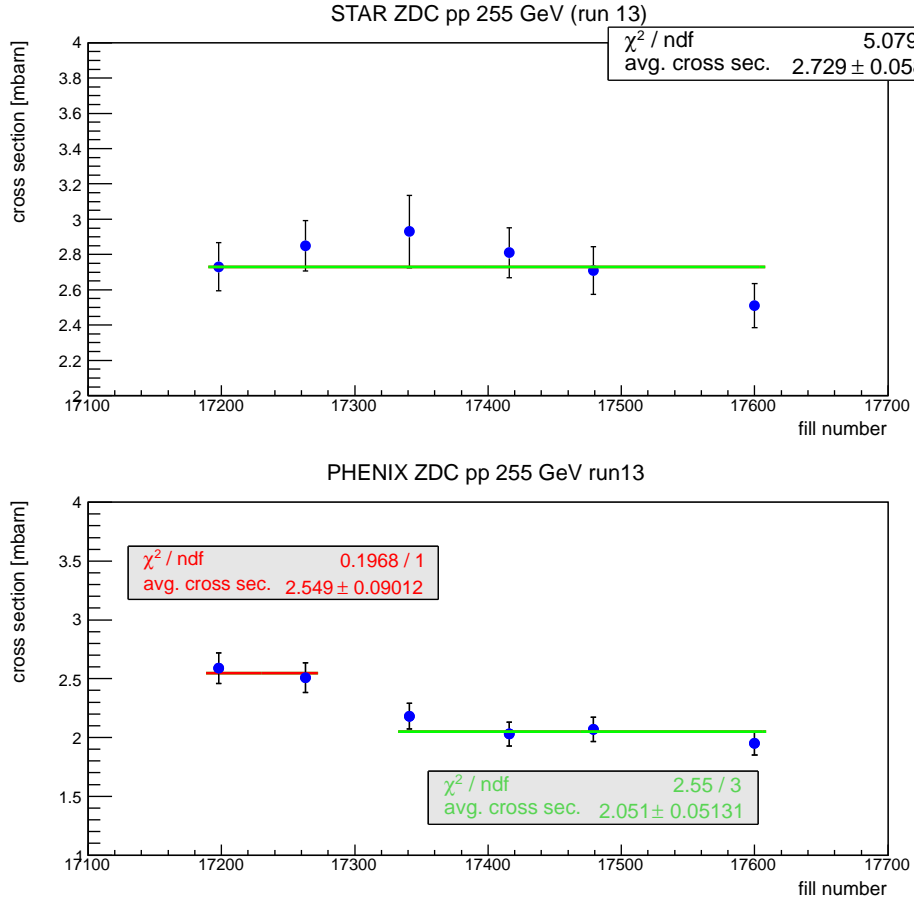


Figure 9: STAR (top) and PHENIX (bottom) ZDC effective cross sections for Run-13.

two IPs if the differences are significant.

It turns out that the first two scans were done with lattice pp13e-s4. For this lattice the  $\beta^*$ -ratio (measured, see [3]) for IP8/IP6 yields 0.914 and most stores had a ratio of colliding bunch pairs of  $107/100 = 1.07$ . Both numbers combined result in an expected

ratio for the two experimental and fully corrected luminosities of 0.98. Note, however, that the measured  $\beta^*$  values for this lattice inherit a larger uncertainty due to fewer data samples available for the analysis. If model values were used the expected ratio would even increase to 1.17, which is equally inconsistent with the vernier scan results. This indicates that the true  $\beta^*$  values are located somewhere between the measured ones and the model.

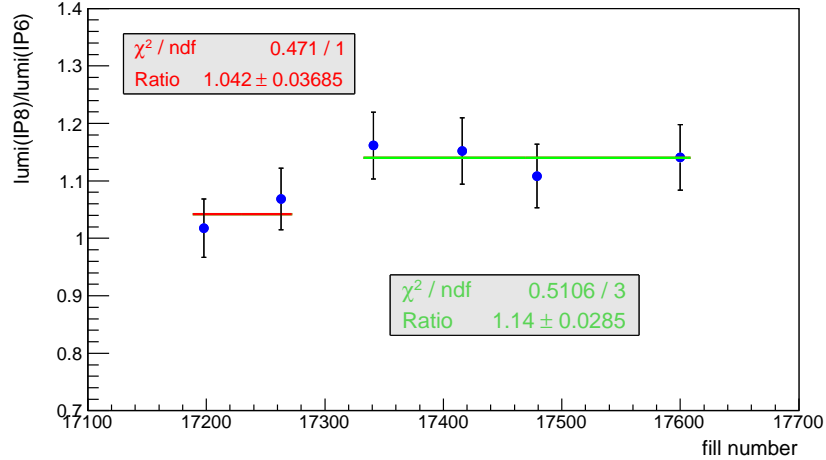


Figure 10: Ratios of measured instantaneous luminosities. Expected values are 0.98 (pp13e-s4) and 1.15 (pp13b-s1). The two lattice periods were fitted separately (pp13e-s4:red and pp13b-s1:green).

The second set of vernier scans, 17341 to 17600, were all done with lattice pp13b-s1. For this lattice the  $\beta^*$ -ratio (measured, see [3]) yields 1.06. Most stores were done with 111/102 pairs of colliding bunches. Both values combined result in an expected ratio for the two experimental and fully corrected luminosities of 1.15. This result is fully consistent with the measurement shown in Figure 10. Note that for this lattice more data samples were available for  $\beta^*$  measurements than for the first one.

Combining the corrections, statistical errors and the systematic errors from above, the resulting effective cross sections for Run-13 are:

**IP6** 2.73 mbarn  $\pm$  2% (stat.)  $\pm$  5% (syst.)

**IP8** before 04/03/13: 2.55 mbarn  $\pm$  3.5% (stat.)  $\pm$  5% (syst.)

after 04/03/13: 2.05 mbarn  $\pm$  2.5% (stat.)  $\pm$  5% (syst.)

We could still gain from an increased number of vernier scans per run.

## References

- [1] A. Baltz et al., Nucl. Instr. and Methods, A417 (1998) 1.
- [2] S. Van Der Meer, ISR-PO/68-31, KEK68-64.

- [3] C. Liu et al., "PRECISION TUNE, PHASE AND BETA FUNCTION MEASUREMENT BY FREQUENCY ANALYSIS IN RHIC.", IPAC13 proceedings, 2013.  
C. Liu, private communication, 2013.
- [4] Ted d'Ottavio, A. Drees, <http://www.cadops.bnl.gov/Controls/doc/lisa/lisa.html>
- [5] K.A.Drees (BNL), S. White (CERN), "Vernier Scan Results from the First RHIC Proton Run at 250 GeV", IPAC10 Proceedings, 2010.
- [6] [http://www.cadops.bnl.gov/Instrumentation/InstWiki/index.php/RHIC\\_Current\\_Transformer](http://www.cadops.bnl.gov/Instrumentation/InstWiki/index.php/RHIC_Current_Transformer)
- [7] D. Cronin-Hennessy, A. Beretvas and P.F. Derwent, "Luminosity monitoring and measurement at CDF", Nucl. Instruments and Methods A433 (2000) 37
- [8] R. Michnoff et al., "RHIC BPM SYSTEM AVERAGE ORBIT CALCULATIONS", PAC proceedings, 2009.
- [9] M.A. Furman, "Hourglass Effects for Asymmetric Colliders", PAC Proceedings, 1991.
- [10] StoreAnalysis application, S. Binello, W. Fischer, private communication
- [11] R. Connolly et al., "RESIDUAL-GAS-IONIZATION BEAM PROFILE MONITORS IN RHIC", Proceedings of BIW10 Conference, Santa Fe, New Mexico, US, 2010.